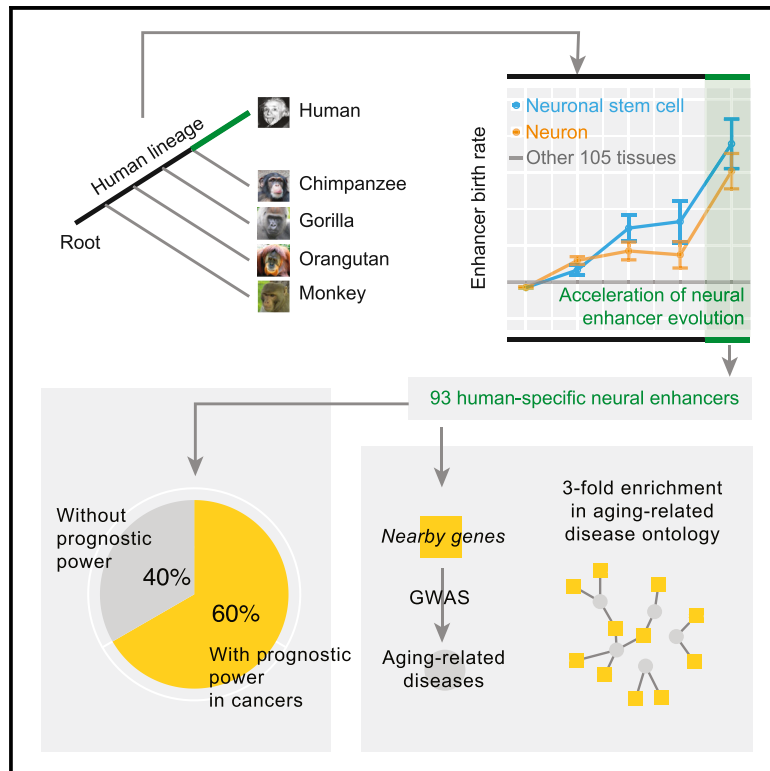**Article**

Fast-Evolving Human-Specific Neural Enhancers Are Associated with Aging-Related Diseases

Graphical Abstract

Authors

Han Chen, Chunyan Li, Zhicheng Zhou, Han Liang

Correspondence

hliang1@mdanderson.org

In Brief

Chen et al. identify ∼100 human-specific enhancers that are activated in neural tissues and were potentially fixed under adaptation. These enhancers are associated with key genes in aging-related diseases such as cancer and Alzheimer's disease.

Highlights

- Identify a group of human-specific enhancers that are activated in neural tissues

- Extensive associations of these enhancers with cancer and other aging diseases

- One such enhancer potentially promotes Alzheimer's disease by counteracting *REST*

- Provide systematic evidence of antagonistic pleiotropy in human evolution

CellPress

Fast-Evolving Human-Specific Neural Enhancers Are Associated with Aging-Related Diseases

Han Chen,[1,4] Chunyan Li,[1,2,4] Zhicheng Zhou,[1,3] and Han Liang[1,3,5,*]

[1]Department of Bioinformatics and Computational Biology, The University of Texas MD Anderson Cancer Center, Houston, TX 77030, USA
[2]Key Laboratory of Genomic and Precision Medicine, China Gastrointestinal Cancer Research Center, Beijing Institute of Genomics, Chinese Academy of Sciences, 100101 Beijing, China
[3]Department of Systems Biology, The University of Texas MD Anderson Cancer Center, Houston, TX 77030, USA
[4]These authors contributed equally
[5]Lead Contact
*Correspondence: hliang1@mdanderson.org
https://doi.org/10.1016/j.cels.2018.04.002

SUMMARY

The antagonistic pleiotropy theory hypothesizes that evolutionary adaptations maximizing the fitness in early age increase disease burden after reproduction. This theory remains largely untested at the molecular level. Here, we analyzed enhancer evolution in primates to investigate the relationships between aging-related diseases and enhancers acquired after the human-chimpanzee divergence. We report a 5-fold increased evolutionary rate of enhancers that are activated in neural tissues, leading to fixation of ~100 human-specific enhancers potentially under adaptation. These enhancers show prognostic expression levels and correlations with driver genes in cancer, and their nearby genes are enriched in known loci associated with aging-related diseases. Using CRISPR/Cas9, we further functionally validated an enhancer on chr8p23.1 as activator counteracting REST, a master regulator known to be a transcriptional suppressor of Alzheimer disease. Our results suggest an evolutionary origin of aging-related diseases: the side effects of human-specific, neural-tissue expressed enhancers. Thus, adaptive molecular changes in human macroevolution may introduce vulnerabilities to disease development in modern populations.

INTRODUCTION

Diseases of aging, such as cancer and Alzheimer, represent a major health burden and are collectively responsible for nearly 90% of deaths nationwide (de Grey, 2007). With longer expected life spans, this burden is increasing. Over recent decades, tremendous efforts have characterized the molecular basis of diseases related to aging in order to develop effective therapies. Advances in high-throughput technologies have enabled systematic approaches to identify hundreds of related vulnerability loci in the human genome (Jeck et al., 2012; Ramos et al., 2014). However, our understanding of the evolutionary origin of aging-related diseases remains very limited (Fabian, 2011).

Along with the cell division limit theory (Weismann, 1889) and mutation accumulation theory (Medawar, 1952), antagonistic pleiotropy is one of the major theories proposed to address the origin of aging-related diseases (Williams, 1957) in which trade-off is the key. As first suggested by Charles Darwin, compromise is inherent in every adaptation as a trade-off (Garland, 2014). George Williams further formulated the hypothesis and argued that if a change caused both increased reproduction in early life and aging in later life, then that change would be adaptive in evolution (Williams, 1957). If true, this theory should particularly apply to the fast adaptations humans have recently experienced, which should be accompanied by a series of trade-offs because of limited evolutionary time for fine-tuning. These trade-offs then would have more profound impacts on the aging-related phenotypes of modern human populations than in any time of macroevolution due to our substantially increased life span over the last two centuries (Finch, 2010) and limited purifying selection, which has been weakened by the use of advanced medications (Fabian, 2011). Following this logic, we hypothesize that the adaptive molecular changes recently acquired in humans may contribute to the development of aging-related diseases. Since the classic paper by King and Wilson in 1975 (King and Wilson, 1975), increasing evidence has indicated that our evolution since the human-chimpanzee divergence has been driven more frequently by changes in gene regulatory elements than in protein sequences (Carroll, 2005; Haygood et al., 2007; Liang et al., 2008; Shi et al., 2006). Therefore, we focused on enhancers, a key class of noncoding regulatory elements (Andersson et al., 2014; Encode Project Consortium, 2012), to test our hypothesis.

RESULTS

Accelerated Evolution Generates Human-Specific Enhancers Activated in Nervous Tissues

Our analysis took advantage of high-resolution, systematic annotation of human tissue-specific enhancers recently available from the FANTOM project (Andersson et al., 2014), which
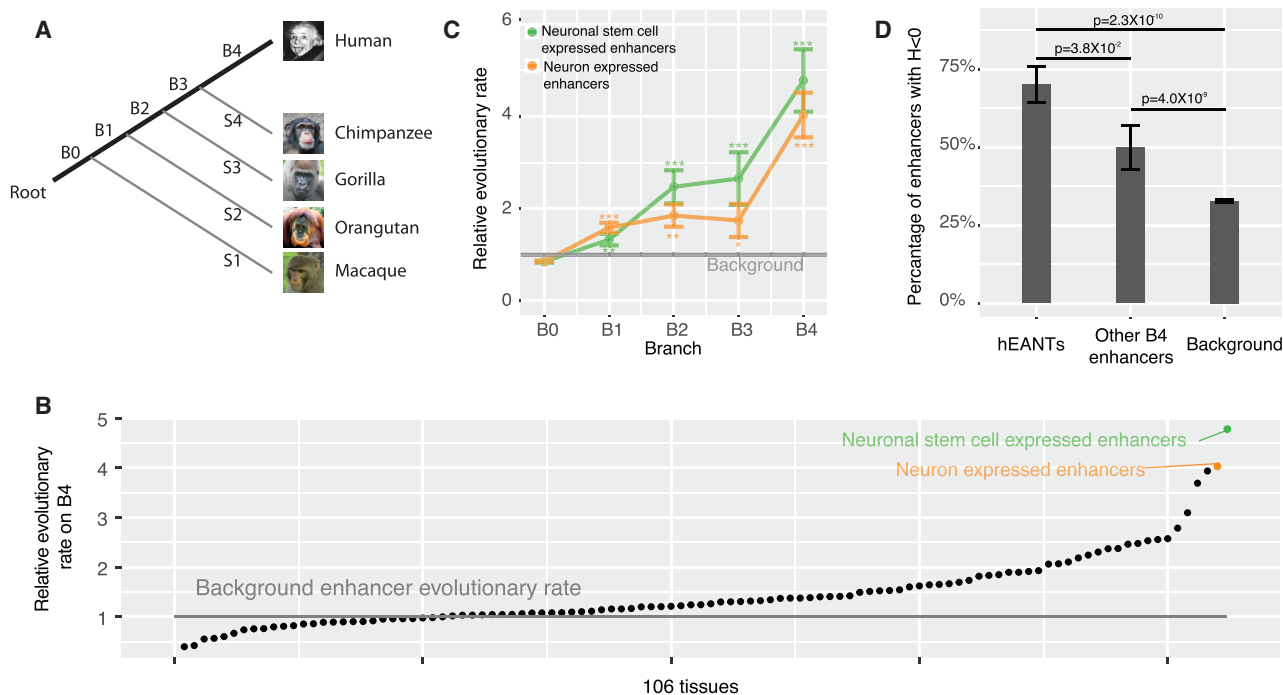
Figure 1. Accelerated Gain of hEANTs during Human-Specific Evolution

(A) The primate phylogeny. B0, ..., B4 donate the branch segments of different evolutionary ages.

(B) Relative B4 evolutionary rate of all tissues. All enhancers (n = 32,748) were categorized to be expressed in one or more of the tissue types annotated by the FANTOM project. Only the tissue types with >100 enhancers were considered (n = 106). The background rate was calculated based on enhancers evolved other than B4.

(C) Accelerated gain of hEANTs in the primate evolution. p values were calculated using a chi-squared test (*p < 0.05, **p < 0.01, and ***p < 0.0001). Error bars represent mean ± SE.

(D) Proportion of enhancers with a negative Fay & Wu's H value (an indication of an excess of high-frequency derived alleles). A chi-squared test was used to compare the difference between any two groups. Error bars represent mean ± SE.

See also Figures S1 and S2 and Tables S1, S2, and S3.

annotated 32,748 enhancers showing tissue-biased expression patterns. We aligned each enhancer to the other four primate genomes (chimpanzee, gorilla, orangutan, and macaque, as shown in Figure 1A) and inferred its origin based on the presence/absence of its orthologs in these primate species (Table S1, STAR Methods). Then, for a given tissue/cell type (n = 106) and a given branch segment (B0, ..., B4) along the phylogenetic tree, we first calculated the proportion of the enhancers expressed in that tissue and evolved in that branch among the ones evolved in that branch, then calculated the proportion of the enhancers expressed in that issue among all the enhancers surveyed, and defined their ratio as the relative evolutionary rate of enhancers (STAR Methods). In this way, we used the birth rate of enhancers in all tissues as the internal control to normalize the effect of branch length, allowing a fair comparison across different tissues. Interestingly, we found that the neuronal stem cell-expressed enhancers and the neuron-expressed enhancers were the two fastest evolving categories on B4, the branch representing human-specific evolution (Figure 1B, Table S2). Because of their similar physiological origins, we combined these two groups of enhancers in the subsequent analyses. The evolution of these enhancers accelerated gradually and reached a >4-fold increased rate after the human-chimpanzee

divergence (B4), suggesting that >75% of the enhancers that evolved on B4 are due to their elevated evolutionary rate. Importantly, this observed pattern remains the same when considering confounding factors (e.g., nucleotide composition, SNP density, and enhancer length) or technical issues (e.g., genome incompleteness and alignment errors) that could potentially compromise the accuracy of our phylogenetic analysis (Chen et al., 2015; Moyers and Zhang, 2016) (Table S3, Figure S1). In total, our analysis revealed 93 non-redundant human-specific enhancers activated in nervous tissues (47 and 66 in neuronal stem cells and neurons, respectively), which hereafter we refer to as hEANTs (Figure 1C, Table S1).

The evolutionary acceleration of hEANTs may be due to relaxed purifying selection or positive selection. We next examined their functional relevance and selective forces. Gene set enrichment analysis indicates that the hEANTs' closest genes are functionally enriched in axon guidance (p = 1.8 × 10^{-5}, false discovery rate [FDR] = 0.01), a critical function for human brain development (Suarez et al., 2014). Since there are no hEANT orthologs in other primate genomes, the common methods for assessing the selective force in macroevolution, such as dN/dS test and McDonald-Kreitman test, could not be applied to these human-specific enhancers. However, given
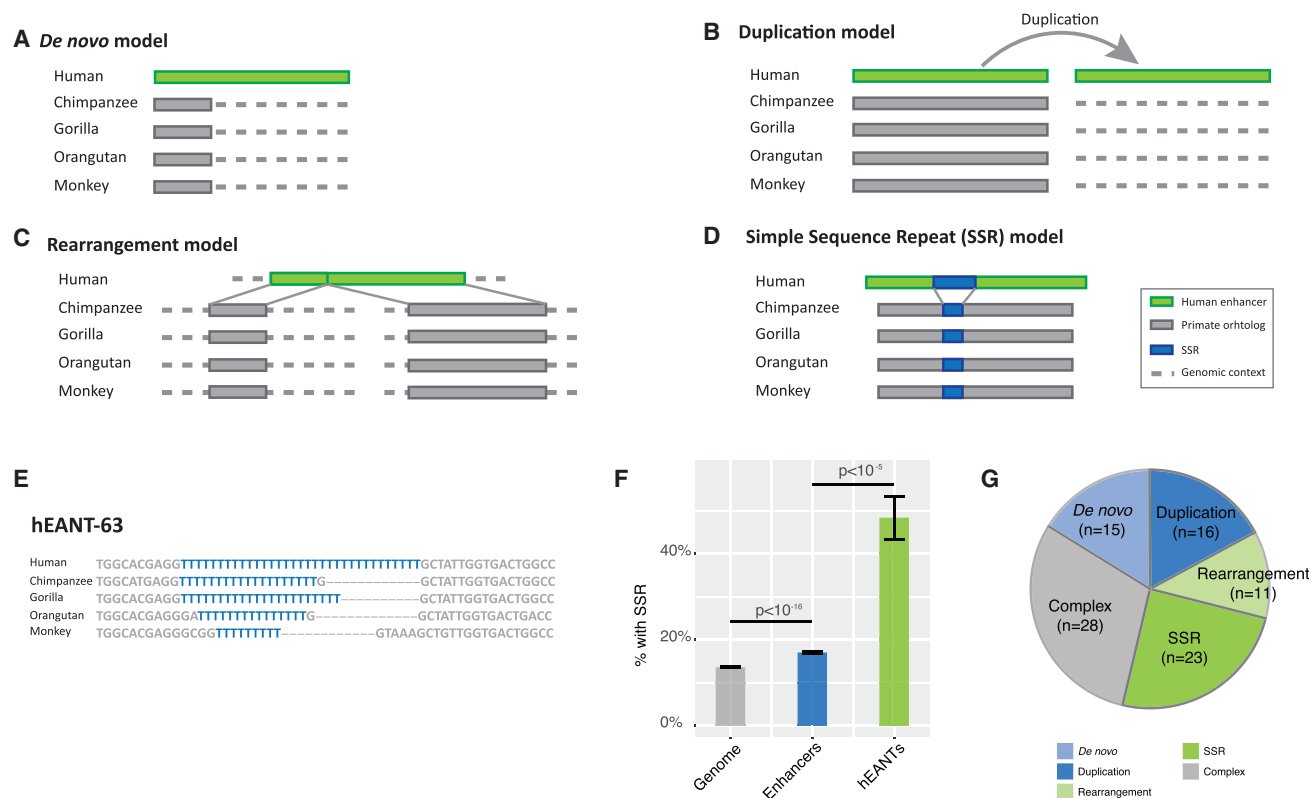
Figure 2. Mechanistic Models of hEANT Origination

(A) *De novo* model.

(B) Duplication model.

(C) Rearrangement model in which an enhancer is created by joining distant genome sequences.

(D) SSR model in which an hEANT evolves through SSR extension.

(E) Alignments of hEANT-63 in the primate lineage.

(F) Enrichment of SSR in the hEANTs. The genome background was calculated by randomly generating pseudo-enhancers with the same length distribution (STAR Methods). p values were calculated with permutation tests for enhancer/background comparison and with chi-squared test for hEANTs/enhancer comparison. Error bars represent SD of sample proportions.

(G) A summary of hEANTs evolved through different models.

that the acceleration trend was observed across the whole human evolution in the primate lineage (Figure 1C), there is a possibility to detect some signals within human populations if some hEANTs were fixed by adaptation recently. For example, the *BRCA1* gene under positive selection after the human-gorilla divergence still shows Hardy-Weinberg disequilibrium in the European population (Huttley et al., 2000). We therefore performed a population genetic analysis based on the 1000 Genomes Project (1000 Genomes Project Consortium et al., 2012) and found that 71% of these hEANTs have negative Fay & Wu's H indexes, a well-established signature of recent positive selection (Fay and Wu, 2000). This proportion is significantly higher than that for other human-specific enhancers or the background enhancers (71% versus 50%, p = 3.8 × 10^{-2}; 71% versus 32%, p = 2.3 × 10^{-10}; Figure 1D), suggesting that positive selection may have played a key role in recruiting the hEANTs into the human genome. Interestingly, this adaptation appeared to be specific to enhancers, as protein-coding genes specifically expressed in the nervous tissues are substantially more conserved than those expressed in other tissues (Figure S2).

Besides the introduction of new enhancers into the human genome, another way to achieve evolutionary innovations is to modify existing enhancers by substitutions. We performed a comparative analysis between human and chimpanzee enhancers using the macaque as the out-group. However, given a very low enhancer substitution rate (dEnhancer = ∼0.003) and an average enhancer length of ∼300 bp, we only detected ∼1.2 human-specific substitutions per enhancer and thus could not identify specific enhancers that may have undergone human-specific acceleration.

Evolutionary Mechanisms of hEANTs

To understand how hEANTs originated during the macroevolution, we searched the homologous/orthologous sequences (orthologous sequences broken or missing according to the UCSC whole-genome alignments) of the 93 hEANTs and their flanking regions (500 bp) in other primate genomes using BLAST. We identified four major models of hEANT origination (Figure 2). (1) *De novo* model: for 15 hEANTs, at least 20% of the enhancer sequences and the corresponding flanking 500 bp regions have no homologous sequence in any of the primate genomes
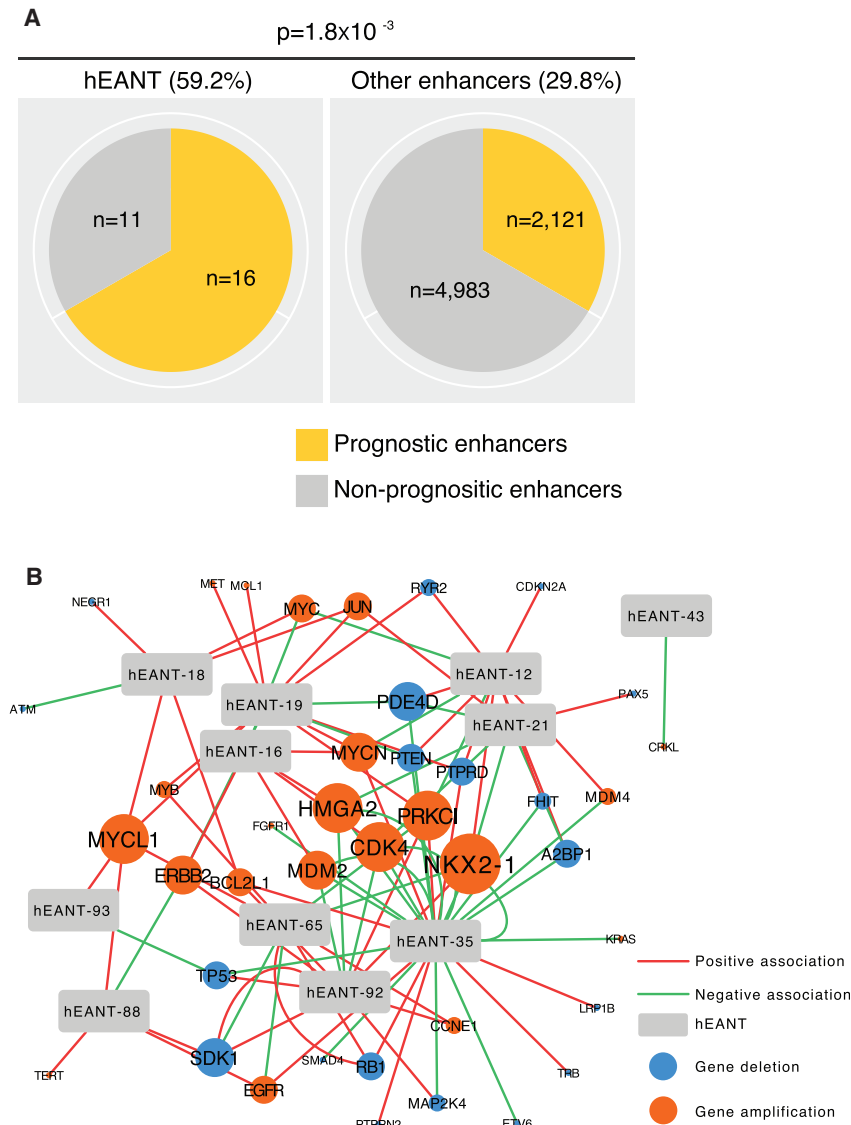
A

p=1.8x10^{-3}

hEANT (59.2%)   Other enhancers (29.8%)

n=11   n=16   n=2,121   n=4,983

🟨 Prognostic enhancers

⬜ Non-prognositic enhancers

B

Positive association
Negative association
⬜ hEANT
🔵 Gene deletion
🟠 Gene amplification

Figure 3. The Association of hEANTs with Cancer

(A) Enrichment of hEANTs in enhancers whose expression levels were significantly correlated with cancer patients' survival times. The analysis only included 7,131 out of the 32,748 enhancers on genomic regions without overlaps with any previously annotated transcriptional events (e.g., genes, lincRNAs, and microRNAs). Prognostically relevant enhancers were identified in at least 1 of the 23 TCGA cancer types surveyed (q < 0.05, Table S4). p value was calculated using a Fisher's exact test.

(B) A network of associations between hEANTs and SCNAs of caner driver genes.

See also Table S4.

Interestingly, previous studies have indicated that SSRs usually locate in regulatory elements (Usdin, 2008), are unstable, and confer hyper-transcriptional evolvability in macroevolution (Vinces et al., 2009) and diversity within the human population (Gymrek et al., 2016). Consistently, we found that the hEANTs strongly enrich SSR, compared with the genome-wide background of all enhancers (Figure 2F), well explaining our findings of accelerated enhancer evolution. Besides the four simple evolutionary models, 28 hEANTs were classified as complex events since they could not be explained by single events, or the homologous sequences were deleted in some primates (Figure 2G).

Association of hEANTs with Aging-Related Diseases

According to the antagonistic pleiotropy theory, we predicted that the hEANTs' trade-offs can cause some deleterious effects on other phenotypic traits and contribute to aging-related diseases. To

(BLAST e < 10^{-10}), indicating their *de novo* origin or gene transfer from species far apart (Figure 2A). (2) Duplication model: consistent with the notion that duplication is a major mechanism through which new genetic elements originate, 16 hEANTs are not the best hits when we BLAST the human genome with their best hits in other primate genomes as inputs, suggesting them to be recent duplications (Figure 2B). This model well explains why they have highly homologous sequences in other primates but no orthologs detected in the whole-genome alignment. (3) Rearrange model: for 11 hEANTs, their orthologs were separated into at least two fragments located separately in the primate genomes (e.g., on different chromosomes), indicating a human-specific rearrangement jointing them into one enhancer (Figure 2C). (4) Simple sequence repeat (SSR) model: we also observed SSR extensions in 23 hEANTs, which are often detected as breaks by the whole-genome alignment (Figure 2D); hEANT-63 serves as a good example of SSR extension in the primate lineage (SSR highlighted in blue Figure 2E).

test this prediction, we first focused on cancer, a major group of aging-related diseases with the most comprehensive genomic data available through The Cancer Genome Atlas (TCGA) (Cancer Genome Atlas Research Network et al., 2013). We used the expression levels of an enhancer calculated from TCGA RNA sequencing data as an approximation of its activity in patient samples (Andersson et al., 2014) since chromatin immunoprecipitation sequencing data are not available for the large patient cohorts. Across 23 TCGA cancer types (Table S4), we focused on 7,131 enhancers with detectable expression and identified the prognostic enhancers, those whose expression was significantly associated with patient survival times (log rank test or univariate Cox model, FDR <0.05; Table S1, STAR Methods). We observed a 2-fold enrichment of prognostic enhancers in the hEANTs relative to all enhancers (59.2% versus 29.8%, Fisher's exact test p = 1.8 × 10^{-3} and binomial test = 1.5 × 10^{-3}; Figure 3A). Indeed, the number of cancer types prognostically associated with an hEANT is much higher than that for
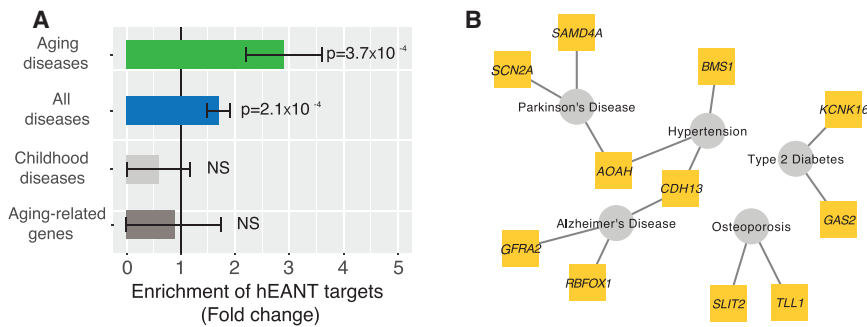
Figure 4. The Association of hEANTs with Other Aging-Related Diseases

(A) Enrichment of hEANTs' closest coding genes in genes associated with aging-related diseases and aging-related genes. Aging-related diseases included Alzheimer disease, Parkinson disease, hypertension, type 2 diabetes, and osteoporosis; childhood diseases included asthma, autism, juvenile arthritis, sickle cell anemia, and type 1 diabetes. For disease association analysis, all genes included in the PheGenI database were used as the background gene set. The list of aging-related genes was obtained from Human Aging Genomic Resources. p value was calculated using a chi-squared test. Error bars represent SD of sample proportions with error prorogation.

(B) A network showing the connections between hEANTs' closest genes and aging-related diseases. See also Tables S5 and S6.

an enhancer otherwise (0.70 versus 0.36, p = 0.013). We also examined the associations between the hEANTs and somatic copy number alterations (SCNAs) of known cancer genes in the TCGA cohorts and identified many associations of hEANTs with the amplifications or deletions of cancer driver genes, such as *TP53*, *PTEN,* and *EGFR,* in multiple cancer types (Figure 3B). Collectively, these results strongly support active roles of hEANTs in cancer development.

To more generally assess the impact of hEANTs on other aging-related diseases, we selected five well-known diseases from the Phenotype-Genotype Integrator (PheGenI) project (Ramos et al., 2014), including Alzheimer disease, Parkinson disease, hypertension, type 2 diabetes, and osteoporosis, and obtained their vulnerability loci identified from related genome-wide association studies. Interestingly, 11 hEANTs' closest genes are associated with the loci identified for these diseases, leading to a 3-fold enrichment (p < 3.7×10^{-4}, Figure 4, Tables S5 and S6). In comparison, there is even a depletion (although not significant) of the hEANTs' closest genes for the susceptibility loci of five typical childhood diseases, including asthma, autism, juvenile arthritis, sickle cell anemia, and type 1 diabetes (Figure 4A). As previously reported, aging-related disease genes and aging-related genes have limited overlaps in most model organisms, indicating their functional differences (Fernandes et al., 2016). Consistently, the hEANTs' closet genes show no enrichment for aging-related genes (Figure 4A), suggesting that their associations with aging-related diseases were not due to the involvement of the general aging process (de Magalhaes et al., 2009).

hEANT-8 Promotes Alzheimer Disease by Counteracting REST

To elucidate the molecular mechanism by which a hEANT plays a critical role in aging-related diseases, we constructed a network of genes co-expressed with each hEANT using the expression data of TCGA brain tumors (i.e., glioblastomas and low-grade glioma, as the brain is the organ in which hEANTs are supposed to function. Interestingly, we identified a well-organized co-expression module containing 121 potential target genes for a hEANT on the 8q23.1 region of chromosome 8 (hereafter referred to as hEANT-8) in both cancer types (Pearson's R > 0.3 and FDR <0.01, STAR Methods, Table S7). We further validated the asso-

ciation between the module expression and hEANT-8 using the GTEx dataset of normal brain tissues (GTEx Consortium, 2015) (Figure 5A). Further analysis of TCGA copy number data revealed that copy number variations of hEANT-8 can lead to module activity changes, suggesting its role as an upstream regulator of the module (Figure S3). This module is associated with a panel of neural or mental diseases (Schriml et al., 2012) (Figure S4). Intriguingly, through the search for motifs enriched on the module genes, we found enrichment of the binding motif of REST (Figure 5B, >24-fold, p < 10^{-16}), a well-studied transcription suppressor in neurons (Schoenherr et al., 1996), indicating the module genes' functional similarity. To further validate its effects on enhancing the module activity, we generated HEK293T cell lines with homozygous hEANT-8 deletion using the CRISPR/Cas9 genetic perturbation system (STAR Methods) and measured the expression levels of 11 module genes positively correlated with the enhancer (Figure 5C; top 11 genes, Table S8). Out of the nine genes with a detectable mRNA expression level, seven genes showed a reduced expression after hEANT-8 deletion, and the reductions in five of them were statistically significant, ranging from 0.60 to 0.85 (Figure 5D). We also observed similar effects in SNB-75, a human brain tumor cell line: six out of the nine hEANT-8 positively correlated genes with a detectable mRNA expression level showed a significant reduction after hEANT-8 deletion (Figure 5E). These results confirmed the causal effects of hEANT-8 on the module activity.

Importantly, *REST* is a key checkpoint for avoiding Alzheimer disease when aging. The loss of the function of this gene in aged brains would abnormally elevate the expression level of its downstream targets, eventually leading to Alzheimer disease (Lu et al., 2014). We found that hEANT-8 showed expression patterns that were the reverse of those of *REST* and their shared targets, suggesting their opposite cellular functions (Figure 6A). Thus, hEANT-8 was predicted to be activated in diseased brains, and indeed this pattern was observed in an independent dataset (Scheckel et al., 2016) (1-tail t test, p < 0.045, Figure 6B). With its reverse effects of *REST*, hEANT-8 may contribute to the susceptibility to Alzheimer disease by abnormally activating the module, which should have been suppressed by *REST* (Figure 6C). These results provide a good illustration of how an hEANT is involved in the pathobiology of an aging-related disease.
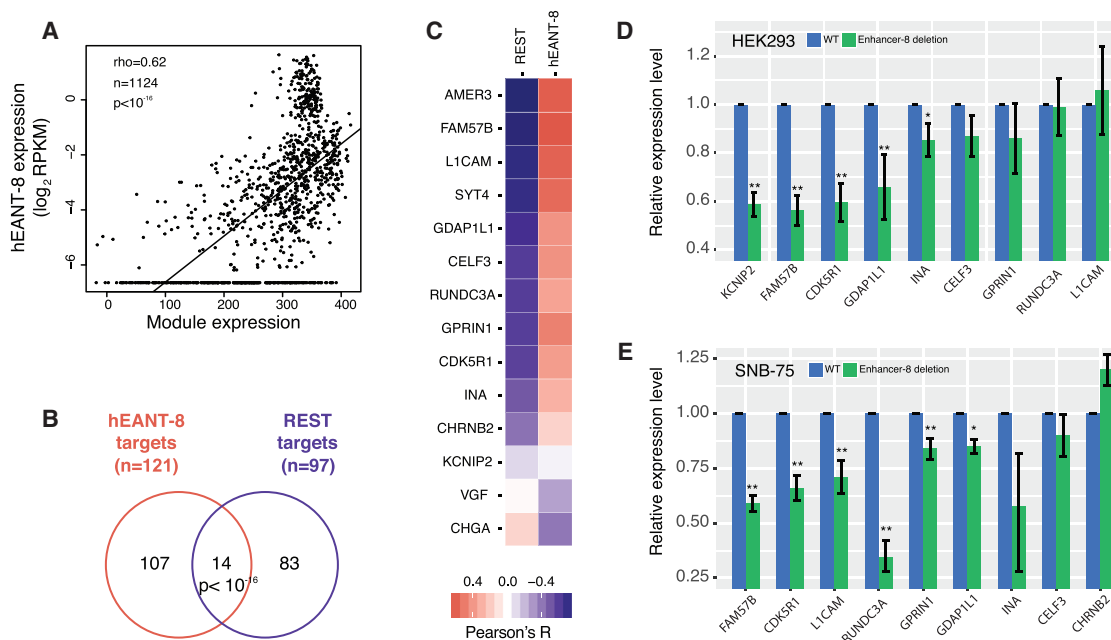
Figure 5. Regulation of hEANT-8 on a Downstream Module Enriched with REST Target Genes

(A) The correlation between hEANT-8 expression and the module expression using the GTEx samples of the central nervous system (n = 1,124). The module's overall expression activity was calculated as the sum of log_2RPKM across all 121 module genes in a sample. The correlation was measured as Spearman's correlation coefficient (rho).

(B) Enrichment of the hEANT-8 target genes (co-expressed module genes) in the REST target genes (genes with a REST binding motif). p value was calculated using a chi-squared test.

(C) Co-expression between hEANT-8 and the 14 genes identified in (B). The colors indicate the correlations with *REST* or hEANT-8 expression level.

(D and E) Expression changes of the nine detectable genes whose expression is positively correlated with hEANT-8 in (C) after its deletion in HEK293T (D) and SNB-75 cells (E). Relative expression levels were calculated as the fold change of the wild-types (WT). Error bars show mean ± SE; p values were calculated by t test with Storey's correction of multiple comparison (*p < 0.05, **p < 0.01).

See also Figures S3 and S4, Tables S7 and S8.

DISCUSSION

George Williams proposed the antagonistic pleiotropic theory that human aging-related diseases originate because natural selection would recruit molecular changes benefiting in the reproductive age even with late-life costs. This theory has not been rigorously tested and its molecular mechanism remains largely unclear, even though some interesting cases of balancing selection have been reported. For example, the *APOE* gene has an allele generating the Apoe4 isoform that benefits young humans with heightened immune response to viruses while contributing to risks of aging-related diseases, such as Alzheimer and higher blood cholesterol (Finch, 2010). A recent systematic analysis on aging-related genes and aging-related disease genes found that for most of the model organisms studied (Fernandes et al., 2016), aging-related genes and aging-related disease genes have few overlaps. The genetic links between aging and aging-related diseases are due to a small fraction of aging-related genes that tend to have a high network connectivity. This finding fits the antagonistic pleiotropic theory well and could be explained as that the general aging process is conducted by the related genes' major functions, while the aging-related diseases are usually associated with the genes' negatively pleiotropic functions. Moreover, the analysis found that while the aging-related genes tend to be more conserved than the overall genome (median

dN/dS = 0.091), the aging-diseases genes show a higher dN/dS ratio (median = 0.137). The higher dN/dS ratio could be explained by either positive selection or relaxation, both of which do not reject the concept of antagonistic pleiotropic.

In the present study, we followed the famous hypothesis of King and Wilson that human adaptations are largely driven by the molecular changes in regulatory elements and tested the antagonistic pleiotropic theory in terms of enhancer evolution. Our study identifies a novel evolutionary mechanism of how aging-related diseases may originate as the trade-off effects of adaptive enhancers recently acquired in human evolution, strongly supporting the theory. Our study links the molecular changes that once conferred some advantages in our long-term evolution with the vulnerability loci that contribute to the development of aging-related diseases in the modern human population, contributing to a deeper understanding of human evolution. Our results have several implications. First, a common practice in biomedical research is to focus on genetic elements with high conservation. But our observation emphasizes the pathological significance of elements newly evolved in our genome when studying aging-related diseases, especially those with a signature of positive selection (e.g., a non-conserved lncRNA). This notion helps prioritize candidate targets for functional and clinical investigations. Second, our study suggests that the genetic network underlying aging-related diseases is
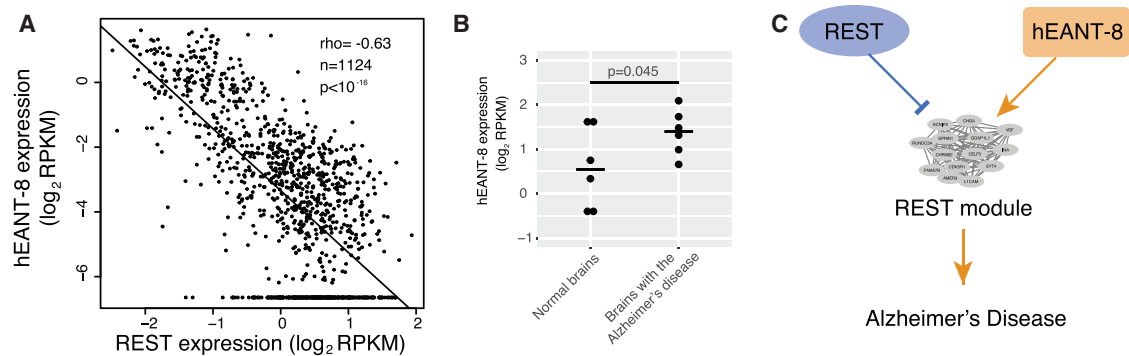
Figure 6. The Role of hEANT-8 in Promoting Alzheimer Disease by Counteracting *REST*

(A) Correlation between hEANT-8 and *REST* using the same data as Figure 5A.

(B) A higher expression of hEANT-8 in diseased tissues (n = 6) than in normal brain tissues (n = 6). p value was based on a one-sided t test.

(C) Schematic representation of the hEANT-8/*REST* counteractions in the development of Alzheimer disease.

perturbed by many molecular changes without being subject to purifying selection after reproductive age, thereby creating complicated epistasis and endless complexity (Chen et al., 2017). This may help to explain the contrasting genetic patterns between many aging-related diseases and Mendelian diseases (Antonarakis and Beckmann, 2006). Finally, because the trade-offs introduced by molecular changes in a gene are not necessarily related to the primary function of the gene, our results suggest that the pleiotropic effects (sub-functions) of a gene, rather than its major function, should be considered when studying aging-related diseases.

STAR★METHODS

Detailed methods are provided in the online version of this paper and include the following:

- KEY RESOURCES TABLE
- CONTACT FOR REAGENT AND RESOURCE SHARING
- EXPERIMENTAL MODEL AND SUBJECT DETAILS
- METHOD DETAILS
  - Evolutionary Rate Analysis of Enhancers
  - Evolutionary Mechanism Analysis of hEANTs
  - Analysis of Cancer Genomic Data
  - Gene Set Enrichment and Disease-Associated Gene Analysis
  - Case Study of hEANT-8 and Alzheimer's Disease
  - CRISPR/Cas9 Perturbation of hEANT-8
- QUANTIFICATION AND STATISTICAL ANALYSIS
- DATA AND SOFTWARE AVAILABILITY

SUPPLEMENTAL INFORMATION

Supplemental Information includes four figures and eight tables and can be found with this article online at https://doi.org/10.1016/j.cels.2018.04.002.

ACKNOWLEDGMENTS

AUTHOR CONTRIBUTIONS

H.L. supervised the whole project. H.C. and H.L. conceived of and designed the research. H.C. and H.L. contributed to the data analysis. C.L. and Z.Z. performed the experiments. H.C., C.L., and H.L. wrote the manuscript, with input from Z.Z.

DECLARATION OF INTERESTS

The authors declare no competing interests.

REFERENCES

1000 Genomes Project Consortium, Abecasis, G.R., Auton, A., Brooks, L.D., DePristo, M.A., Durbin, R.M., Handsaker, R.E., Kang, H.M., Marth, G.T., and McVean, G.A. (2012). An integrated map of genetic variation from 1,092 human genomes. Nature *491*, 56–65.

Andersson, R., Gebhard, C., Miguel-Escalada, I., Hoof, I., Bornholdt, J., Boyd, M., Chen, Y., Zhao, X., Schmidl, C., Suzuki, T., et al. (2014). An atlas of active enhancers across human cell types and tissues. Nature *507*, 455–461.

Antonarakis, S.E., and Beckmann, J.S. (2006). Mendelian disorders deserve more attention. Nat. Rev. Genet. *7*, 277–282.

Benson, G. (1999). Tandem repeats finder: a program to analyze DNA sequences. Nucleic Acids Res. *27*, 573–580.

Braak, H., and Braak, E. (1991). Neuropathological staging of Alzheimer-related changes. Acta Neuropathol. *82*, 239–259.

Cancer Genome Atlas Research Network, Weinstein, J.N., Collisson, E.A., Mills, G.B., Shaw, K.R., Ozenberger, B.A., Ellrott, K., Shmulevich, I., Sander, C., and Stuart, J.M. (2013). The Cancer Genome Atlas Pan-Cancer analysis project. Nat. Genet. *45*, 1113–1120.

Carroll, S.B. (2005). Evolution at two levels: on genes and form. PLoS Biol. *3*, e245.

Chen, H., Lin, F., Xing, K., and He, X. (2015). The reverse evolution from multi-cellularity to unicellularity during carcinogenesis. Nat. Commun. *6*, 6367.

Chen, H., Wu, C.I., and He, X. (2017). The genotype-phenotype relationships in the light of natural selection. Mol. Biol. Evol. https://doi.org/10.1093/molbev/msx288.

Encode Project Consortium (2012). An integrated encyclopedia of DNA elements in the human genome. Nature *489*, 57–74.

Fabian, D., and Flatt, T. (2011). The evolution of aging. Nature Education Knowledge *3*, 9.

Fay, J.C., and Wu, C.I. (2000). Hitchhiking under positive Darwinian selection. Genetics *155*, 1405–1413.

Fernandes, M., Wan, C., Tacutu, R., Barardo, D., Rajput, A., Wang, J., Thoppil, H., Thornton, D., Yang, C., Freitas, A., et al. (2016). Systematic analysis of the gerontome reveals links between aging and age-related diseases. Hum. Mol. Genet. *25*, 4804–4818.

Finch, C.E. (2010). Evolution in health and medicine Sackler colloquium: evolution of the human lifespan and diseases of aging: roles of infection, inflammation, and nutrition. Proc. Natl. Acad. Sci.USA *107* (*Suppl 1*), 1718–1724.

Garland, T. (2014). Trade-offs. Curr. Biol. *24*, R60–R61.

de Grey, A.D.N.J. (2007). Life span extension research and public debate: societal considerations. Stud. Ethics, Law, Technol. *1*, https://doi.org/10.2202/1941-6008.1011.

GTEx Consortium (2015). Human genomics. The Genotype-Tissue Expression (GTEx) pilot analysis: multitissue gene regulation in humans. Science *348*, 648–660.

Gymrek, M., Willems, T., Guilmatre, A., Zeng, H., Markus, B., Georgiev, S., Daly, M.J., Price, A.L., Pritchard, J.K., Sharp, A.J., et al. (2016). Abundant contribution of short tandem repeats to gene expression variation in humans. Nat. Genet. *48*, 22–29.

Haygood, R., Fedrigo, O., Hanson, B., Yokoyama, K.D., and Wray, G.A. (2007). Promoter regions of many neural- and nutrition-related genes have experienced positive selection during human evolution. Nat. Genet. *39*, 1140–1144.

Huttley, G.A., Easteal, S., Southey, M.C., Tesoriero, A., Giles, G.G., McCredie, M.R., Hopper, J.L., and Venter, D.J. (2000). Adaptive evolution of the tumour suppressor BRCA1 in humans and chimpanzees. Australian Breast Cancer Family Study. Nat. Genet. *25*, 410–413.

Jeck, W.R., Siebold, A.P., and Sharpless, N.E. (2012). Review: a meta-analysis of GWAS and age-associated diseases. Aging cell *11*, 727–731.

King, M.C., and Wilson, A.C. (1975). Evolution at two levels in humans and chimpanzees. Science *188*, 107–116.

Li, J., Han, L., Roebuck, P., Diao, L., Liu, L., Yuan, Y., Weinstein, J.N., and Liang, H. (2015). TANRIC: an interactive open platform to explore the function of lncRNAs in cancer. Cancer Res. *75*, 3728–3737.

Liang, H., Lin, Y.S., and Li, W.H. (2008). Fast evolution of core promoters in primate genomes. Mol. Biol. Evol. *25*, 1239–1244.

Locke, D.P., Hillier, L.W., Warren, W.C., Worley, K.C., Nazareth, L.V., Muzny, D.M., Yang, S.P., Wang, Z., Chinwalla, A.T., Minx, P., et al. (2011). Comparative and demographic analysis of orang-utan genomes. Nature *469*, 529–533.

Lu, T., Aron, L., Zullo, J., Pan, Y., Kim, H., Chen, Y., Yang, T.H., Kim, H.M., Drake, D., Liu, X.S., et al. (2014). REST and stress resistance in ageing and Alzheimer's disease. Nature *507*, 448–454.

de Magalhaes, J.P., Curado, J., and Church, G.M. (2009). Meta-analysis of age-related gene expression profiles identifies common signatures of aging. Bioinformatics *25*, 875–881.

Medawar, P.B. (1952). An Unsolved Problem of Biology (H.K. Lewis).

Mootha, V.K., Lindgren, C.M., Eriksson, K.F., Subramanian, A., Sihag, S., Lehar, J., Puigserver, P., Carlsson, E., Ridderstråle, M., Laurila, E., et al. (2003). PGC-1alpha-responsive genes involved in oxidative phosphorylation are coordinately downregulated in human diabetes. Nat. Genet. *34*, 267–273.

Moyers, B.A., and Zhang, J. (2016). Evaluating phylostratigraphic evidence for widespread de novo gene birth in genome evolution. Mol. Biol. Evol. *33*, 1245–1256.

Ramos, E.M., Hoffman, D., Junkins, H.A., Maglott, D., Phan, L., Sherry, S.T., Feolo, M., and Hindorff, L.A. (2014). Phenotype-Genotype Integrator (PheGenI): synthesizing genome-wide association study (GWAS) data with existing genomic resources. Eur. J. Hum. Genet. *22*, 144–147.

Rosenbloom, K.R., Armstrong, J., Barber, G.P., Casper, J., Clawson, H., Diekhans, M., Dreszer, T.R., Fujita, P.A., Guruvadoo, L., Haeussler, M., et al. (2015). The UCSC Genome Browser database: 2015 update. Nucleic Acids Res. *43*, D670–D681.

Scheckel, C., Drapeau, E., Frias, M.A., Park, C.Y., Fak, J., Zucker-Scharff, I., Kou, Y., Haroutunian, V., Ma'ayan, A., Buxbaum, J.D., et al. (2016). Regulatory consequences of neuronal ELAV-like protein binding to coding and non-coding RNAs in human brain. Elife *5*, https://doi.org/10.7554/eLife.10421.

Schoenherr, C.J., and Anderson, D.J. (1995). The neuron-restrictive silencer factor (NRSF): a coordinate repressor of multiple neuron-specific genes. Science *267*, 1360–1363.

Schoenherr, C.J., Paquette, A.J., and Anderson, D.J. (1996). Identification of potential target genes for the neuron-restrictive silencer factor. Proc. Natl. Acad. Sci. USA *93*, 9881–9886.

Schriml, L.M., Arze, C., Nadendla, S., Chang, Y.W., Mazaitis, M., Felix, V., Feng, G., and Kibbe, W.A. (2012). Disease ontology: a backbone for disease semantic integration. Nucleic Acids Res. *40*, D940–D946.

Shi, P., Bakewell, M.A., and Zhang, J. (2006). Did brain-specific genes evolve faster in humans than in chimpanzees? Trends Genet. *22*, 608–613.

Simao, F.A., Waterhouse, R.M., Ioannidis, P., Kriventseva, E.V., and Zdobnov, E.M. (2015). BUSCO: assessing genome assembly and annotation completeness with single-copy orthologs. Bioinformatics *31*, 3210–3212.

Suarez, R., Gobius, I., and Richards, L.J. (2014). Evolution and development of interhemispheric connections in the vertebrate forebrain. Front. Hum. Neurosci. *8*, 497.

Subramanian, A., Tamayo, P., Mootha, V.K., Mukherjee, S., Ebert, B.L., Gillette, M.A., Paulovich, A., Pomeroy, S.L., Golub, T.R., Lander, E.S., et al. (2005). Gene set enrichment analysis: a knowledge-based approach for interpreting genome-wide expression profiles. Proc. Natl. Acad. Sci. USA *102*, 15545–15550.

Tacutu, R., Thornton, D., Johnson, E., Budovsky, A., Barardo, D., Craig, T., Diana, E., Lehmann, G., Toren, D., Wang, J., et al. (2017). Human ageing genomic resources: new and updated databases. Nucleic Acids Res. *46*, D1083–D1090.

Usdin, K. (2008). The biological effects of simple tandem repeats: lessons from the repeat expansion diseases. Genome Res. *18*, 1011–1019.

Vinces, M.D., Legendre, M., Caldara, M., Hagihara, M., and Verstrepen, K.J. (2009). Unstable tandem repeats in promoters confer transcriptional evolvability. Science *324*, 1213–1216.

Weismann, A. (1889). Essays upon Heredity and Kindred Biological Problems (Clarendon Press).

Williams, G.C. (1957). Pleiotropy, natural selection, and the evolution of senescence. Evolution *11*, 398–411.

Yu, G., Wang, L.G., Yan, G.R., and He, Q.Y. (2015). DOSE: an R/Bioconductor package for disease ontology semantic and enrichment analysis. Bioinformatics *31*, 608–609.

STAR★METHODS

KEY RESOURCES TABLE

REAGENT or RESOURCE	SOURCE	IDENTIFIER
Deposited Data		
Reference genomes (hg19, PanTro4, GorGor3, PonAbe2, and Rh3Mac3)	UCSC Genome Browser	http://hgdownload.soe.ucsc.edu/downloads.html: RRID: SCR_005780
TCGA RNA-seq BAM files	Genomic Data Commons	https://portal.gdc.cancer.gov/legacy-archive/search/f: RRID: SCR_014514
TCGA somatic copy number alteration thresholded data	Firehose Broad GDAC	https://gdac.broadinstitute.org/
TCGA gene expression data	Firehose Broad GDAC	https://gdac.broadinstitute.org/
TCGA patient clinic data	cBioPortal	http://www.cbioportal.org/: RRID: SCR_014555
FANTOM enhancer annotation	(Anderson et al., 2014)	http://fantom.gsc.riken.jp/5/datafiles/latest/extra/Enhancers/human_permissive_enhancers_phase_1_and_2.bed: RRID:SCR_002678
Genome completeness data	(Simao et al., 2015)	http://busco.ezlab.org/: RRID: SCR_015008
1000 genome project SNP data	1000 Genomes Project Consortium et al., 2012	http://www.1000genomes.org/data#download: RRID: SCR_006828
Phenotype–Genotype Integrator (PheGenI) database	(Ramos et al., 2014)	https://www.ncbi.nlm.nih.gov/gap/phegeni
The Alzheimer's Disease RNA-seq dataset	(Scheckel et al., 2016)	https://www.ncbi.nlm.nih.gov/geo/query/acc.cgi?acc=GSE53697
GTEx RNA-seq dataset	dbGAP	https://www.gtexportal.org/home/: RRID: SCR_013042
Software and Algorithms		
LiftOver	UCSC Genome Browser	https://genome.ucsc.edu/cgi-bin/hgLiftOver
Samtools	(Li et al., 2009)	http://samtools.sourceforge.net/: RRID: SCR_002105
Tandem Repeats Finder	(Benson, 1999)	https://tandem.bu.edu/trf/trf.html
Disease ontology analysis	(Yu et al., 2015)	https://www.bioconductor.org/packages/3.7/bioc/vignettes/DOSE/inst/doc/DOSE.html
Fay & Wu H-test	(Fay and Wu, 2000)	http://www.genetics.wustl.edu/jflab/htest.html
Gene Set Enrichment Analysis (GSEA)	(Mootha et al., 2003; Subramanian et al., 2005)	http://software.broadinstitute.org/gsea/index.jsp: RRID: SCR_003199
Experimental Models: Cell Lines		
HEK293T	MD Anderson Characterized Cell Line Core Facility	HEK293T; RRID:CVCL_0063
SNB-75	MD Anderson Characterized Cell Line Core Facility	SNB75
Oligonucleotides		
sgRNA-L2 target: CCTCTTCTTCCACCTCCCCG	This study	NA
sgRNA-L3 target: ACTCCCGGTCTCCACGGCTT	This study	NA
sgRNA-R1 target: CGCAGAAGTGCGCTCCACGA	This study	NA
sgRNA-R2 target: TAGGTCTGATGTCCGCGGGA	This study	NA
sgRNA-R3 target: GAAAGACACAAACACCGCCA	This study	NA
5' PCR primer for detecting hEANT-8 deletion: GCTGAGGTCGAGCTCCTTTT	This study	NA

(Continued on next page)

Continued		
REAGENT or RESOURCE	SOURCE	IDENTIFIER
3′ PCR primer for detecting hEANT-8 deletion: AAATGGCCTCGAAGCGAGAA	This study	NA
PCR primer sequences for hEANR-8 coexpression module genes	This study	Table S8
Recombinant DNA		
pSpCas9(BB)-2A-GFP (PX458)	This study	Addgene: Plasmid #48138
pU6-(BbsI)CBh-Cas9-T2A-mCherry	This study	Addgene: Plasmid #64324

CONTACT FOR REAGENT AND RESOURCE SHARING

Further information and requests for resources and reagents should be directed to and will be fulfilled by the Lead Contact, Han Liang (hliang1@mdanderson.org).

EXPERIMENTAL MODEL AND SUBJECT DETAILS

HEK (human embryonic kidney) 293T cell line and SNB-75 cell line were obtained from the Characterized Cell Line Core Facility (CCLC) at MD Anderson Cancer Center. Both cell lines were fingerprinted by short tandem repeat (STR) DNA profiling at CCLC. The sex of these two cell lines were female. HEK293T cells and the cell lines established based on HEK293T were cultured in Dulbecco's modification of Eagle's medium (DMEM) with 10% fetal bovine serum (Invitrogen) at 37°C and 5% CO_2. SNB-75 cells and the cell lines established from SNB-75 were maintained in RPMI-1640 with 10% fetal bovine serum at 37°C and 5% CO_2.

METHOD DETAILS

Evolutionary Rate Analysis of Enhancers

The FANTOM project annotated the expression patterns of enhancers in the human genome (Andersson et al., 2014). We obtained 32,748 enhancers showing a tissue-specific expression pattern from http://enhancer.binf.ku.dk/presets/facet_expressed_enhancers.tgz. Using the UCSC whole genome alignment chain files (which considered the synteny and orientation) and the liftOver tool, we aligned these enhancers to four primate genomes, including the chimpanzee (*Pan troglodytes*, PanTro4), gorilla (*Gorilla gorilla*, GorGor3), orangutan (*Pongo pygmaeus abelii*, PonAbe2) and monkey (*Macaca mulatta*, RheMac3) (Rosenbloom et al., 2015). The primate phylogeny is ((((Human, Chimpanzee), Gorilla), Orangutan), Monkey) (Locke et al., 2011). Enhancers unmapped by the liftOver were considered as missing in a genome of interest. We then defined the origin of an enhancer on the deepest branch ahead of the last common ancestry that descended to all species with its ortholog. For example, an enhancer only aligned to the gorilla genome was considered to originate on B2 (Figure 1A). Table S1 provides the evolutionary ages (branch) of all 32,748 enhancers. For the given tissue TY and branch BX, the relative evolutionary rate was calculated as the ratio of the proportion of TY enhancers on BX to the proportion of enhancers expressed in TY among all enhancers. We only considered the tissue or cell types with >100 enhancers (n = 106). We combined the neuronal stem cell expressed enhancers (FANTOM ID CL:0000047) and neuron expressed enhancers (CL:0000540) and termed them as enhancers activated in nervous tissue (EANT). EANTs evolved on B4 were referred to as human-specific ENATs, or hEANTs. Table S2 provides the details about the calculation of relative evolutionary rates in Figures 1B and 1C.

We used the analysis of covariance (ANCOVA) to study the dependency of evolutionary age on a series of factors, including EANT tissue type, GC content, enhancer length, and expression level. The evolutionary age was the response variable, where 1 was for enhancers on B4 or 0 for otherwise. The independent variable included tissue type (1 for EANTs or 0 for otherwise), GC content, SNP density and enhancer length. SNP density was calculated based on the 1000 Genomes Project (1000 Genomes Project Consortium et al., 2012). The other factors were transformed into Z scores first. The ANCOVA was performed using the R package *anova*. We also considered the effects of genome completeness and false alignments. The genome completeness data were obtained from the BUSCO database (Simao et al., 2015). We artificially introduced a 10% false positive/negative alignment rate by randomly adding/removing 10% of the human enhancers missed/present in each of the four genomes. The resulting data were used to recalculate a relative evolutionary rate on B4. This procedure was repeated 100 times to estimate the impact of a 10% false alignment rate on our results.

We used SNP allele frequencies in the 1000 Genomes Database to detect positive selection on the enhancers. Specifically, we obtained from the reference genome, for each enhancer, a 2-kb sequence in which the enhancer is located in the middle. The allele frequencies of all SNPs on this sequence were calculated using the 1000 Genomes Project VCF files (http://www.1000genomes.org/data#download) and then subjected to Fay & Wu's H-index calculation (Fay and Wu, 2000). For the H-index, the simulation was performed using the default settings (http://www.genetics.wustl.edu/jflab/htest.html).

For each protein-coding gene, we measured its conservation level as the (1-dN/dS) after the human orangutan divergence (the rhesus and orangutan orthologs were used to infer the ancestry status), where dN/dS represents the ratio of the number of non-synonymous substitutions per non-synonymous site (dN) to the number of synonymous substitutions per synonymous site (dS). Only genes with alignment >100 amino acids and dS >0.01 (n = 16,001) were considered to ensure the accuracy of the conservation calculation. For each of the 54 GTEx tissues, we measured a given gene's expression bias as the ratio of its expression ($\log_2$RPKM) in the tissue to its median level across all tissues. We sorted all the protein-coding genes by their conservation and evenly divided them into 100 groups. Then we calculated the means of conservation and expression bias for genes in these groups and examined the correlation (Pearson's R in Figure S2) between the genes' conservation levels and their expression bias in a tissue.

Evolutionary Mechanism Analysis of hEANTs

Since the LiftOver tool could not provide detailed information on how the hEANTs originated, we searched the hEANTs and their flanking 500 bp sequences in the four primate genomes using BLAST in order to examine their evolutionary mechanisms. We used the e-value of 10^{-25} as the cutoff of positive BLAST results and manually curated all BLAST results in the following five steps. (1) We classified the hEANTs (n = 15) without BLAST results in the primate genomes as *De novo* model (Figure 2A). (2) We determined hEANTs (n = 11) generated by rearrangement as indicated by their flanking sequences being BLAST to separated genomic regions in the primate genomes (Figure 2B). (3) For the other hEANTs, we picked their best hits in the four primate genomes and blasted them back in the human genome. If none of the best hits in the human genome was the hEANT itself, we classified it as duplication model (n = 16; Figure 2C). (4) We subjected the remaining hEANTs to Tandem Repeats Finder (TRF; default settings; https://tandem.bu.edu/trf/trf.html) for SSR identification. For 23 hEANTs with SSRs in all the genomes involved, we manually aligned them and found that all these hEANTs have their SRRs extended in the human genome, explaining why they could not be mapped to the primate genomes by LiftOver. Thus, they were classified as SSR model (Figures 2D and 2E). (5) The remaining 28 hEANTs could not be explained by any simple model and usually involved more than one of the four models, thereby being classified as complex model (Figure 2G). We calculated the SSR rate of hEANTs, total enhancers, and the genome background using TRF with default settings. The genome background was calculated by randomly generating pseudo-enhancers (n = 32748) with the same length distribution for 100 times.

Analysis of Cancer Genomic Data

For enhancer expression analysis, we first re-annotated the 32,748 FANTOM enhancers according to the UCSC gene annotation file (refgene.txt) and removed the enhancers that overlapped with known genes or intron regions, resulting in a subset of 7,131 enhancers for which the RNA-seq reads can be confidently assigned (Table S1). We obtained TCGA RNA-seq BAM files from UCSC CGHub and our dataset contained >8,000 tumor samples of 23 cancer types. We obtained patient survival data from the Broad Firehose website, from which 8,380 samples have available overall patient survival data and 6,837 samples have progression-free survival data for the analysis (Cancer Genome Atlas Research Network et al., 2013) (Table S4). We calculated the RPKM values of the enhancers in TCGA samples as previously described (Li et al., 2015). For each cancer type, we further filtered enhancers without detectable expression in >10% of the samples. For each cancer type, we identified prognostic enhancers (overall survival or progression-free survival) using the Cox-regression model and the log-rank test. In the analysis, q < 0.05 (John Storey's correction) in any cancer type were considered statistically significant.

For the SCNA-enhancer association analysis, we obtained the copy number information of 586 cancer driver genes (Cancer Gene Census) in 8,948 tumors of 23 cancer types. The association between a hEANT expression and a CGC gene was examined using Spearman's rank correlation within each cancer type. Significant correlations were identified (q < 0.01; John Storey's correction) in a given cancer type.

Gene Set Enrichment and Disease-Associated Gene Analysis

We identified the nearest coding gene for each of the 93 hEANTs and pooled them as the input for enrichment set. Gene set enrichment analysis was based on the online tools on GSEA website (http://software.broadinstitute.org/gsea/index.jsp), using the default setting (Subramanian et al., 2005). Gene set collections included in this analysis were CP:BIOCARTA, CP:KEGG and CP:REACTOME. For hEANTs-disease analysis on Figure 4, we first obtained a gene-disease association network in the PheGenI database (Ramos et al., 2014), from which we manually selected (i) five typical aging-related diseases, including Alzheimer's disease, Parkinson's disease, hypertension, type-II diabetes, and osteoporosis; and (ii) five childhood diseases as a control, including asthma, autism, juvenile arthritis, sickle cell anemia and type-I diabetes. The aging-related gene list was obtained from Human Ageing Genomic Resources (Tacutu et al., 2017). We used a chi-squared test to compare hEANT neighbor genes with known genes associated with these two groups of diseases to determine the significance of the enrichment. Tables S5 and S6 provide the data related to this section.

Case Study of hEANT-8 and Alzheimer's Disease

We constructed hEANT co-expression networks using TCGA glioblastoma (GBM) and low grade glioma (LGG) datasets (Table S4). For each hEANT, we identified genes co-expressed (absolute Pearson R > 0.3 and FDR < 0.01) in both datasets to form a hEANT-centered co-expression module. We found 121 co-expressed genes for the hEANT-8 on chr8:9764051-9764441, while no other hEANT had a module size of >5 (Table S7). Disease ontology analysis on the hEANT-8 module was based on the R package

DOSE using the default setting (Figure S4) (Schriml et al., 2012; Yu et al., 2015). We further obtained 1,124 samples of different brain regions from the GTEx dataset to validate the co-expression module (GTEx Consortium, 2015). The overall activity of the module (the x axisx axis in Figure 5A) in a given sample was calculated as the sum of all genes' $\log_2$RPKM values. For the copy number analysis in Figure S3, we classified the patients by the copy number of hEANT-8, where patients with <0.9, 0.9~1.1 and >1.1 copies of hEANT-8 were grouped respectively as copy number loss, copy number neutral and copy number gain. The overall activity of the module was calculated as previously described. For the motif analysis, the REST target genes were obtained from the GSEA database under the gene set ID V\$NRSF_01 which was curated from previous studies (Schoenherr and Anderson, 1995; Schoenherr et al., 1996). To compare the hEANT-8 expression between normal and diseased brains, we obtained the dataset from the GEO (accession number, GSE53697) (Scheckel et al., 2016). The original dataset contains brain samples representing different pathological stages of Alzheimer's disease (AD) from a normal condition to serious AD. We filtered two samples from patients of extremely old age ($\geq$100 years). For the remaining samples, six with Braak stage = 0 were used as the normal control group, while six with Braak stage $\geq$5 were used as the disease group (Braak and Braak, 1991). We used Student's t-test to assess if the expression of hEANT-8 is higher in the disease group.

CRISPR/Cas9 Perturbation of hEANT-8

We designed 2/3 gRNA sequences using Cas-Designer (http://www.rgenome.net/cas-designer/) within 150 bp sequences up/down-stream of hEANT-8, generating 6 gRNA combinations. We chose up/down-stream gRNA targeting the genomic sequence CCTCTTCTTCCACCTCCCCG/ CGCAGAAGTGCGCTCCACGA to generate hEANT-8 deletion clones. The up/down stream gRNAs were cloned into cas9 plasmid (Addgene 48138/64324) with GFP/mCherry as reporters. In day 0, each combination of gRNAs was transfected, using lipofectamin 3000, into HEK293T cells grown in Dulbecco's modified Eagle's medium (DMEM) or SNB-75 cells (human brain origin) grown in RPMI-1640, both with 10% fetal bovine serum (Invitrogen) at 37°C and 5% CO_2. In the day 3, the cells were collected for gRNA efficiency examination using genomic PCR. We transfected the gRNA plasmid mixture, and then sorted the GFP/mCherry positive single cells into 96-well plates two days after transfection using MoFlo Astrios Cell Sorters (Beckman Coulter, for HEK293T cells), or three days after transfection using BD FACSAria II Cell Sorter (BD Biosciences, for SNB-75 cells) for colony expansion. The hEANT-8 deletion clones were examined using genomic PCR after ~1 month (HEK293T cells) or ~2 months (SNB-75 cells). Their RNAs were extracted using RNeasy Plus Mini Kit (Qiagen), and 1 μg (for HEK293T cells) or 2 μg (for SNB-75 cells) total RNAs were reversely transcribed into cDNA with High Capacity cDNA Reverse Transcription Kit (Thermo Fisher Scientific). qRT-PCR was performed with SYBR Select master mix (Thermo Fisher Scientific) and in Mastercycler RealPlex (Eppendorf). Table S8 lists the qRT-PCR primer sequences of hEANT-8 target genes. For HEK293T cells, we obtained 4 single-cell clones with homologous hEANT-8 deletion, and for each single-cell clone, 3~4 experimental replicates were carried out; and for each gene in each replicate, qRT-PCR measurements were repeated for 3 times. For SNB-75 cells, we obtained one single-cell clone with heterozygous hEANT-8 deletion, and for each gene, qRT-PCR measurements were repeated for 4 times. For both HEK293T and SNB-75 cell, 2 out of the 11 hEANT-8 positively correlated genes had a baseline expression level lower than our qRT-PCR detection limit (Ct > 40) and were excluded from the analysis.

QUANTIFICATION AND STATISTICAL ANALYSIS

The definitions of significance for the various statistical tests are described and referenced in the respective Method Details sections.

DATA AND SOFTWARE AVAILABILITY

Data and Software availability are described in Key Resources Table.